Int. J. Radiation Oncology Biol. Phys., Vol. 71, No. 5, pp. 1553–1562, 2008

0360-3016/08/$–see front matter

ELSEVIER

doi:10.1016/j.ijrobp.2008.04.017

**PHYSICS CONTRIBUTION**

# EVIDENCE THAT MR DIFFUSION TENSOR IMAGING (TRACTOGRAPHY) PREDICTS THE NATURAL HISTORY OF REGIONAL PROGRESSION IN PATIENTS IRRADIATED CONFORMALLY FOR PRIMARY BRAIN TUMORS

ANITHA PRIYA KRISHNAN, M.S.,* ISAAC M. ASHER,† DELPHINE DAVIS, PH.D.,†‡ PAUL OKUNIEFF, M.D.,† AND WALTER G. O'DELL, PH.D.*†

Departments of *Biomedical Engineering, †Radiation Oncology, and ‡Imaging Sciences, University of Rochester, Rochester, NY

**Purpose:** Stereotactic radiotherapy (SRT) is fast becoming the method of choice for treatment of nonsuperficial brain lesions. SRT treatment plans of malignant brain tumors typically incorporate a 20-mm isotropic margin to account for microscopic tumor spread; however, distant or progressive tumors occur outside this margin. Our hypothesis is that paths of elevated water diffusion may provide a preferred route for transport or migration of cancer cells. If our hypothesis is correct, then future SRT treatment volumes could be modified to provide elongated treatment margins along the paths of elevated water diffusion, thereby creating a biologically better treatment plan that may reduce the incidence of progression.

**Methods and Materials:** Magnetic resonance diffusion tensor imaging (DTI) datasets were acquired on patient subjects before the appearance of >5 mm diameter progressive lesions or secondary tumors. DTI was performed using an echo-planar imaging sequence on a 1.5T clinical General Electric scanner with voxel dimensions of 0.98 × 0.98 × 6 mm. After SRT, patients were given repeated magnetic resonance imaging follow-ups at regular intervals to identify early tumor progression. When progressive disease was detected, DTIstudio and FMRIB Software Library software was used to compute paths of preferred water diffusion through the primary tumor site and the site of progression.

**Results:** Our preliminary results on 14 patient datasets suggest a strong relationship between routes of elevated water diffusion from the primary tumor and the location of tumor progression.

**Conclusions:** Further investigation is therefore warranted. Future work will employ more sophisticated fiber analysis in a prospective study. © 2008 Elsevier Inc.

**Diffusion tensor imaging, Tractography, Stereotactic radiotherapy, Treatment margins, Brain tumor.**

## INTRODUCTION

Approximately 17,000 new cases of primary brain cancer are diagnosed in the United States annually (1). Several common types of primary brain cancer have a historical and physiologic basis for aggressive tumor spread in the brain that thwarts our most sophisticated technology and all existing pharmacologic agents. These include oligodendrogliomas, low-grade astrocytomas, anaplastic astrocytomas, and glioblastomas. With current chemotherapy and radiation techniques, the 5-year survival rate for patients older than age 45 ranges from 16% for those with anaplastic astrocytomas to 2% or less for those with glioblastomas (2). High-dose stereotactic radiotherapy (SRT) is a relatively new treatment technology that can be used to deliver a lethal dose of radiation to a small target site with rapid dose falloff into the surrounding normal tissue to minimize the side effects of harmful radiation to normal tissue (3–6). High dose conformal RT, including SRT, is fast becoming the method of choice for treatment of nonsuperficial brain lesions.

A typical SRT treatment plan for a high-grade astrocytoma includes a uniform margin of up to 25 mm surrounding the lesion to account for any unobserved microscopic spread of tumor cells. This margin size is based on histologic analysis of maximal tumor spread at autopsy dating from the 1980s (7). Because there are no means to directly observe microscopic tumor spread *in vivo*, the same margin size is used in all directions (isotropic) unless there is a need to avoid critical structures in the brain. Unfortunately, the use of large

Reprint requests to: Walter G. O'Dell, Ph.D., Department of Radiation Oncology, University of Rochester, Medical Center, 601 Elmwood Avenue, Box 647, Rochester, NY 14642. Tel: (585) 273-4103; Fax: (585) 275-1531; E-mail: wodell@rochester.edu

Conflict of interest: none.

Funding for portions of this work was provided through a grant from the Gateway for Cancer Research (formerly the Cancer Treatment Research Foundation) and the Rochester Center for Brain Imaging.

*Acknowledgments*—The authors wish to acknowledge insightful discussions and data interpretations from Drs. Sven Ekholm, Jianhui Zhong, and Tong Zhu from the Departments of Imaging Sciences and Biomedical Engineering at the University of Rochester.

Received Oct 30, 2007, and in revised form March 24, 2008. Accepted for publication April 18, 2008.

isotropic margins leads to unnecessary ablation of healthy brain tissue, resulting in cognitive dysfunction, whereas the margins are too small in some regions, leading to tumor progression, often with catastrophic results. The goal of this study is to use magnetic resonance (MR) diffusion tensor imaging (DTI) to predict the microscopic spread of aggressive brain tumors and to help us better understand the mechanisms of tumor spread. These enhancements could then lead to improved anisotropic margins for radiation treatment of malignant brain tumors that would achieve greater local cancer control and increased patient survival while potentially decreasing harmful side effects associated with radiation therapy by reduction of margins in low-risk regions.

Our scientific hypothesis is that migrating brain cancer cells follow the paths of least resistance as determined from MR DTI. This hypothesis is supported by the following observations. First, in areas of white matter, the direction of greatest diffusion usually parallels the predominant underlying fiber orientation and it is known from postmortem studies in humans that glioma cancer cells that migrate the greatest distance from primary tumor sites are located predominantly along white matter tracts (8–11). Second, Jacobsen *et al*. (12) observed that, during embryogenesis, neonatal astrocytes show a preferential movement along developing axon tracts.

II

If cell migration were to occur in an isotropic medium, then there would be an equal probability of spread in all directions; however, it is known that diffusion of water in the brain is highly anisotropic. The local anisotropic diffusion of water molecules in the brain can be measured noninvasively *in vivo* using MR DTI (13–21). The local diffusion coefficient along any predefined direction can be quantified using a standard MR imaging sequence augmented with a pair of diffusion encoding gradients. The local three-dimensional diffusion environment is expressed by the diffusion tensor and the process of computing the diffusion tensor at each voxel in the image is DTI. DTI tractography is the process by which the voxel-wise values of the diffusion tensor are used to estimate the paths that water will travel from one voxel to the next. In the brain, the paths of greatest diffusion are found to parallel the neuronal fiber tracts. Thus when applied in regions of white matter, DTI tractography can be used to reconstruct the local nerve fiber architecture (13, 16–18).

Tractography is commonly realized using either streamline or probabilistic approaches. The streamline approach is also commonly referred to as deterministic tractography. In the streamline approach, the reconstructed tract through each voxel runs parallel to the voxel's principal diffusion direction defined as the eigen vector corresponding to the largest eigen value of the $3 \times 3$ diffusion tensor (15, 19–21). Knowledge of the direction from the previous step and of the diffusion directions in adjacent voxels is often incorporated into the algorithm to achieve a more reasonable and reproducible solution. Streamlined methods typically assume one dominant fiber direction per voxel and hence fail in instances of fiber crossing. Probabilistic tractography incorporates the uncertainty associated with the diffusion parameters into an estimate of the probability of connection between two points (14). The advantage of such probabilistic methods is that they can be more robust to noise when the difference between the magnitude of the diffusion tensor eigen values is small (*i.e*., when the fractional anisotropy value is small) and can therefore track fibers within gray matter and where multiple nonparallel fiber bundles are present within a single voxel.

## METHODS AND MATERIALS

### *Patient selection*

Data were collected for patients who were treated for aggressive gliomas with SRT at the University of Rochester Medical Center and who had documented tumor progression and where the progression was entirely or mainly outside of the original planning target volume. On identification of a potential subject, the patient's medical image database was examined for the presence of a DTI dataset that was acquired before the diagnosis of progressive disease. The DTI datasets used for analysis were typically acquired around the time of SRT planning. The protocol inclusion criteria required there to be DTI data acquired before the presence of extensive progressive disease that could potentially alter the diffusion environment that was present at the time when the first wave of migratory cancer cells was active (22). No other factors were taken into account when selecting patient datasets for analysis. The protocol was approved by the institutional Internal Review Board according to federal and institutional guidelines. Three categories of patients were defined. Category 1 (Distant Secondary Tumor Group) included Patients 1–5 who had secondary tumors located greater than 2 cm beyond the SRT treatment volume. Category 2 (local secondary tumor group) included patients 3 and 6–11 who had secondary tumors within 2 cm or on the boundary of the treatment plan and had no sign of progression in the DTI dataset. Category 3 (progression group) included patients 12–14 who had surgical resection followed by SRT and progression on or near the margin of the primary tumor.

### *Image acquisition*

The datasets were acquired using a clinical whole-body 1.5 Tesla (1.5T) scanner (General Electric SIGNA EXCITE, Milwaukee, WI) as part of the standard of care imaging protocol in place at the authors' institution. After an initial acquisition of axial and coronal T1 and T2 weighted anatomic images with voxel dimensions $0.98 \times 0.98 \times 3$ mm, DTI was performed using one of the following echo-planar imaging sequences using the following parameters: *(1)* TR 10 s; echo time 89.4 ms; 20 serial axial slices; 25 diffusion gradient directions and three reference scans ($b = 0$) scans; and voxel dimensions of $0.98 \times 0.98 \times 6$ mm; or *(2)* repetition time 10.8 s; echo time 101.3 ms; 38 axial slices; 21 diffusion gradient directions and two reference scans and voxel dimensions of $0.94 \times 0.94 \times 3$ mm. As per standard of care, after SRT, patients were given repeated MR image follow-ups at regular intervals to identify early progressive disease. When progressive disease was detected, DTI data acquired before SRT were processed using DTIStudio and FMRIB Software Library (FSL) software to compute all paths of preferred water diffusion through the primary tumor site. In the analyses shown, all fiber pathways from the area of tumor are depicted, although the complete three-dimensional fiber architecture is often not fully appreciated when viewing is limited to two-dimensional projections.

*DTIStudio*

A streamline tractography approach was employed using DTIStudio, made available by Mori *et al.* (from http://lbam.med.jhmi.edu/DTIuser/DTIuser.asp). DTIStudio uses fiber assignment by continuous tracking, a streamline tractography technique demonstrated by Huang *et al.* (18). DTIStudio was implemented such that tracking was initiated from every voxel in the brain MR dataset and was stopped when the fractional anisotropy value became less than 0.2. Tracking was also terminated when the angle between the principal direction in one voxel and that of the next voxel exceeded a cut-off of 70°. DTIStudio was used to identify all diffusion paths that passed through the primary tumor, defined as the observable contrast enhancing mass on a T1-weighted MR imaging dataset.

*FSL*

A probabilistic tractography approach using the software package FSL was created by Behrens *et al.* (14) (available from http://www.fmrib.ox.ac.uk/fsl/le). For this study, the MR imaging DICOM files were converted into analyze format using MRIcro by C. Rorden (http://www.sph.sc.edu/comd/rorden/mricro.html). Brain tissue was segmented using Brain Extraction Tool, a part of the software package FSL, and a brain mask was created. FSL was used to identify all high-probability diffusion paths that passed through the primary tumor, as determined from the T1-weighted MRI dataset.

## RESULTS

*Category 1 (distant secondary tumor group)*

To demonstrate the results for Category 1 patients, Fig. 1 presents the processed image data of Patient 1 with a glioblastoma multiforme (GBM) in the splenium of the corpus callosum (Fig. 1A) and progressive disease on the genu of the corpus callosum (Fig. 1D). Using DTIStudio for analysis and display, two prominent fiber tracts were found to pierce the treatment margin anteriorly, one on each side of the central ventricle (Fig. 1C). These correspond to the internal capsules and the progression is coincident with the path of the prominent left fiber bundle.

For Patient 2, the primary tumor was an oligoastrocytoma in the lower to mid-temporal lobe and the secondary tumor seen 9 months later was in the corpus callosum near the splenium (Fig. 2A, 2B). A preponderance of diffusion paths from the primary tumor site passed directly to the secondary tumor (Fig. 2C, 2D).

The primary tumor of Patient 3 was a GBM in the right frontal lobe; the secondary tumor seen 11 months later was in the left frontal lobe. The fibers passing through the primary tumor reconstructed using DTIStudio and the genu of corpus callosum directly connected the primary and secondary tumor sites.

Patient 4 showed a pattern of cancer spread to the midline of the genu of the corpus callosum following treatment of a primary GBM located in the splenium of the corpus callosum, similar to Patient 1. However, when using both FSL and DTIStudio to reconstruct the paths there were no apparent diffusion paths directly connecting or passing through the primary and secondary tumor locations in this patient.

Patient 5 had a gliomatosis cerebri in the left temporal lobe and the secondary tumor seen 6 months later was in the left parietal-occipital lobe, one slice superior to the primary tumor. The location of both the tumors was best visualized in the coronal images. The fibers passing though the primary tumor reconstructed using both DTIStudio and FSL showed no fibers directly connecting the primary and secondary tumor sites.

*Category 2 (local secondary tumor group)*

In the category wherein the secondary tumor site was within 2 cm of the treatment margin, the sixth patient's original tumor was a GBM of approximately a 2-cm radius located in the left posterior frontal lobe (Fig. 3A) and the secondary tumor was lateral, posterior, and one slice (3 mm) superior (Fig. 3D). Because the primary tumor was located in the gray matter, there was insufficient diffusion anisotropy to enable DTIStudio to reconstruct the fiber architecture. FSL was therefore used to reconstruct the diffusion paths for this patient. The SRT treatment plan is shown in Figure 3B and the green curve outlines the 80% isodose volume. This isodose is indicated by the pink curve in Fig. 3A, 3C, and 3D. When applying FSL to the pretreatment DTI dataset, we found that the probability maps of diffusion paths indicated the presence of a prominent path extending beyond the tumor margin posteriorly and medially (Fig. 3C). The T1-weighted postcontrast images obtained 3 months after SRT showed a secondary tumor that had developed just beyond the treatment site (Fig. 3D) in the region approximately coincident with the diffusion path extension computed from the pretreatment DTI dataset (Fig. 3C).

The primary tumor of Patient 7 was an astrocytoma in the right temporal lobe. The DTI dataset for this patient was obtained 8 months post-SRT treatment. The secondary tumor observed 19 months later, was three slices superior to the primary tumor near the ventricles in the right temporal lobe, only a few millimeters away from the treatment margin and best visualized in the coronal images. The probability maps of diffusion paths generated using FSL showed the presence of prominent paths connecting the primary and secondary tumor sites.

In Patient 8, the primary tumor was an anaplastic astrocytoma located in the left temporal lobe (Fig. 4A). Diffusion paths passing through the tumor were determined using DTIStudio (Fig. 4C). Two major diffusion paths pierced the treatment volume: one directed anteriorly and one posteriorly from the primary tumor. The secondary tumor (Fig. 4D) observed 3 months later was located along the posterior diffusion path. Figure 4E illustrates a hypothetical anisotropic treatment plan that was designed by increasing the dose margin 2 cm along the two prominent diffusion paths and reducing the dose margin given to the surrounding normal tissue. Had this new anisotropic treatment plan been applied to this patient, the secondary tumor may have been prevented (Fig. 4F), for it does indeed lie on the prominent posterior diffusion path that was originally seen at the time of treatment (Fig. 4C). At the same time, damage to normal tissue may have been reduced in the lateral regions where the treatment margin is reduced.

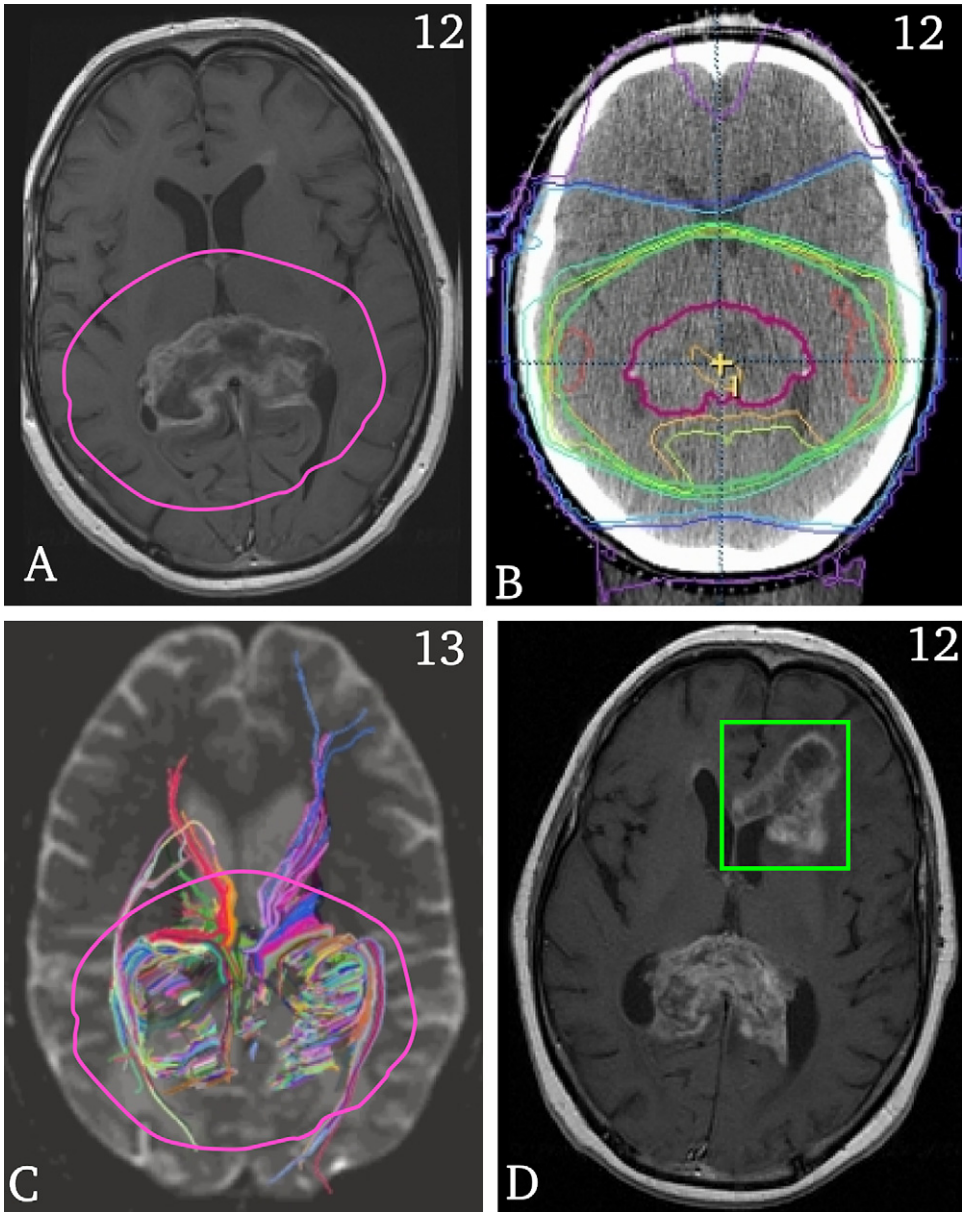


Fig. 1. (A) T1 weighted postcontrast magnetic resonance image acquired 6 months after SRT showing a previously stereotactic radiotherapy treated primary glioblastoma multiforme (GBM) in the splenium of corpus callosum. (B) Treatment margins of the primary GBM overlaid onto the computed tomography planning image. The 90% isodose volumes are shown by pink lines on other images (light green in this image and pink in C). (C) Diffusion tensor imaging reference image (b = 0) at the same time point of (A) showing all the tracts from the primary tumor projected on the two-dimensional plane, as determined using DTIStudio. Tracts do not course significantly superoinferiorly. Four bundles of tracts pierce the treatment margin, where the two most prominent correspond to the inner capsules. (D) T1 weighted postcontrast image of the secondary tumor (green box) 3 months after the time point of (A), which occurred along the most prominent piercing tract in (C).

Patient 9 had an oligoastrocytoma in the right temporal lobe and two secondary tumors. Secondary tumor one was seen 7 months later posterior to the primary tumor; secondary tumor two was seen 17 months later after secondary tumor one. Secondary tumor two was posterior to both the primary tumor and initial secondary tumor. The DTI dataset for this patient was obtained 3 months posttreatment of the primary tumor. The fibers passing through the primary tumor were reconstructed using DTIStudio and both secondary tumors seemed to lie on the same major fiber bundle, the external capsule.

The primary tumor of Patient 10 was an anaplastic astrocytoma in the left frontal lobe. The secondary tumor was posterior to the primary tumor and was seen approximately 3 years later. For this patient DTI datasets were available both pre and post-SRT treatment and the posttreatment images were used for analysis because there was edema in the pretreatment images. The fibers passing through the primary tumor

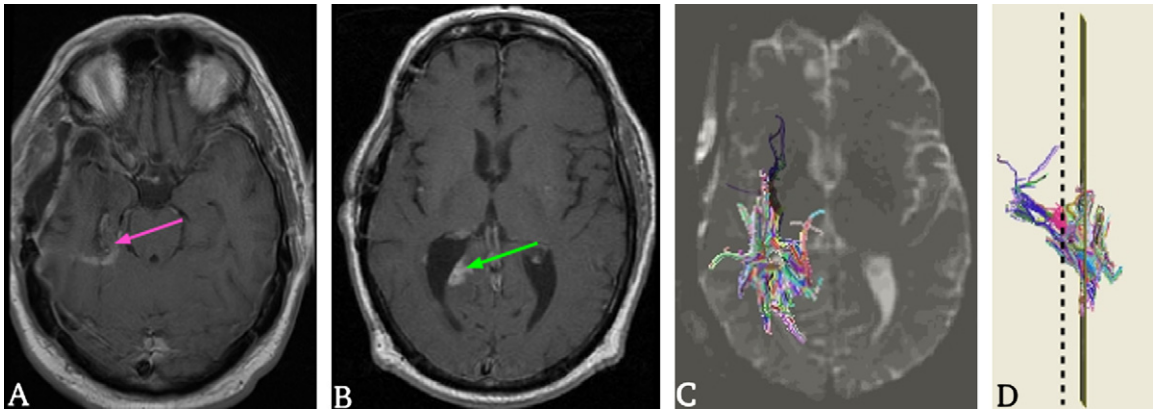


Fig. 2. (A) T1-weighted postcontrast image showing the location of a primary oligoastrocytoma (pink arrow) in the lower to mid-temporal lobe. (B) T1-weighted postcontrast image 9 months after (A) of a secondary tumor (green arrow) in the splenium of corpus callosum, two slices superior to the primary tumor. (C) Diffusion tensor imaging reference image (b = 0) at the initial time point when the primary tumor was observed showing tracts from the primary tumor determined using DTIStudio projected onto the two-dimensional plane of the secondary tumor. (D) Side view of the reconstructed fibers showing intersection with the slice corresponding to the location of the primary tumor and with the slice corresponding to the location of the secondary tumor (dotted line).

were reconstructed using DTIStudio and the secondary tumor was found to lie along the internal capsule.

Patient 11 had a primary GBM in the right parietal-occipital lobe and a secondary tumor seen approximately 3 years later one slice inferior to the primary tumor. The fibers passing though the primary tumor reconstructed using both DTIStudio and FSL showed no fibers directly connecting the primary and secondary tumor sites.

Patient 3 also had a local secondary tumor seen 7 months later that was posterior to the primary GBM in the right frontal lobe, thus rendering Patient 3 under both categories 1 and 2. The fibers passing through primary tumor were determined using DTIStudio and the secondary tumor was along the external capsule.

*Category 3 (Progression Group)*

Patients 12 and 13 were both treated initially using a combination of surgical resection and SRT. Patient 12 had continued primary tumor growth on the border of the resection site. The primary tumor was a GBM in the right frontal lobe and the progression seen 8 months later was near the longitudinal fissure, and later spreading to the left frontal lobe (Fig. 5A, 5D). Most diffusion paths passing through the tumor corresponded to a part of the genu of the corpus callosum and were directed medially toward the site of progression. The distal extensions of the diffusion paths also matched the future spread of progressive disease (Fig. 5C). Diffusion paths were also calculated from the site of progression. These paths corresponded to the uncinate fasciculus, the internal capsule, and other known fiber bundles.

The primary tumor of Patient 13 was an oligoastrocytoma in the right temporal lobe, near the skull (Fig. 6A). Diffusion paths were found to course predominantly anteroposteriorly, with little deviation superiorly, and inferiorly and with a slight curvature towards the center of the brain (corresponding to intersecting fibers of the corpus callosum and the internal capsule; Fig. 6B). The progressive disease seen 2 months later began to be visible posterior to the primary tumor, but quickly spread to encompass a large portion of the right hemisphere (Fig. 6C).

In Patient 14, the primary tumor was a low grade astrocytoma in the right frontal lobe. The tumor was resected initially followed by radiotherapy. It recurred 5 months later along the anterior and inferior surgical cavity, which was treated using radiotherapy. The tumor continued to grow along the fiber tracts passing through the primary tumor 11 months later (T1-weighted images). The diffusion paths passing through the primary tumor were determined using DTIStudio; they correlated well with the direction of spread of the tumor.

Additional analysis was performed on Patient 1 who was unique in that at the time of the earliest available DTI he presented with a very early instance of progression. The T1-weighted image of this patient obtained at 6 months post-SRT treatment (Fig. 7A) showed a small (<5 mm diameter) hyperintense region in the anterior horn of the left lateral ventricle. For this special case, diffusion paths emanating from the site of enhancement were also computed and are depicted in Fig. 7B. The tracts from the site of enhancement course laterally and anteriorly, corresponding to fibers of the genu of corpus callosum, internal capsule, and uncinate fasciculus. At the time, the region of enhancement was noted as suspicious by the attending physicians, but was not diagnosed as an instance of progressive disease. Because of its small size, it was decided that the presence of this early stage of progression would not significantly alter the diffusion environment. Subsequent T1-weighted images of the same patient obtained an additional 3 months later (Fig. 7C) show the spread of the secondary tumor, with substantial growth both laterally and anteriorly. The macroscopic growth pattern around the secondary tumor site was also coincident

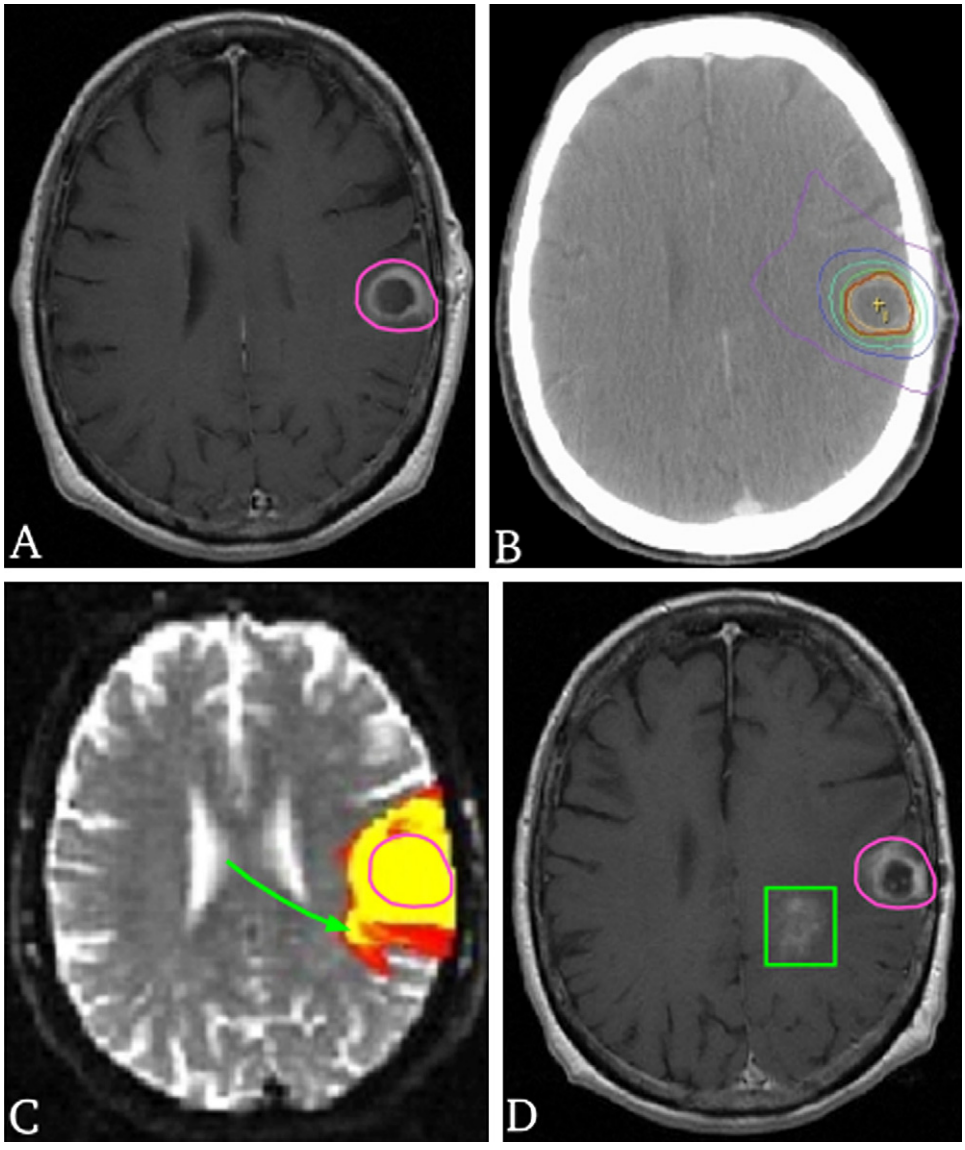


Fig. 3. (A) T1-weighted image showing a ~2 cm glioblastoma multiforme. (B) Computed tomography image used for stereotactic radiotherapy (SRT) treatment planning showing the 100% isodose curve (yellow), the 80% isodose contours (green), the observable tumor (red), and a 4–6 mm treatment margin (green line). Because of the location of tumor, a treatment margin of approximately 4–6 mm instead of 2 cm was used. Pink lines on the other images correspond to the 80% isodose volume. (C) Probability maps of tracts leading from the border of the primary tumor, determined using FMRIB's Diffusion Toolbox in the FMRIB Software Library. Tracts with high relative probability are indicated by yellow and those with moderate probability are indicated by red. A prominent tract is seen extending beyond the treatment margin posteriorly and medially (green arrow). (D) T1-weighted image at 3 months post-SRT shows a secondary tumor (green box) developed just beyond the treatment site, in the region approximately coincident with the tract extension (C).

with the dominant diffusion paths passing through the site of the secondary tumor, primarily along the genu of corpus callosum and uncinate fasciculus (Fig. 7C).

## DISCUSSION

The present study examines the use of MR DTI in predicting patterns of secondary tumor growth and tumor progression. This was done to determine if the natural history of progressive disease can be predicted from microscopic tumor spread as foreseen by DTI, thus validating a new approach to defining individual anisotropic radiation treatment plans.

There were definitive diffusion paths going from the tumor to the secondary or site of progression in eleven out of fourteen patients. In Category 1 patients (distant secondary tumor group), the original and secondary tumors both lie on opposite ends of a known white matter tract in the inner capsule. Perhaps the internal capsule is distinctive in some respect from other white matter tracts or the tract is altered by the tumor itself, causing the tumor cells to migrate and spread more often along this particular tract. It is also possible that

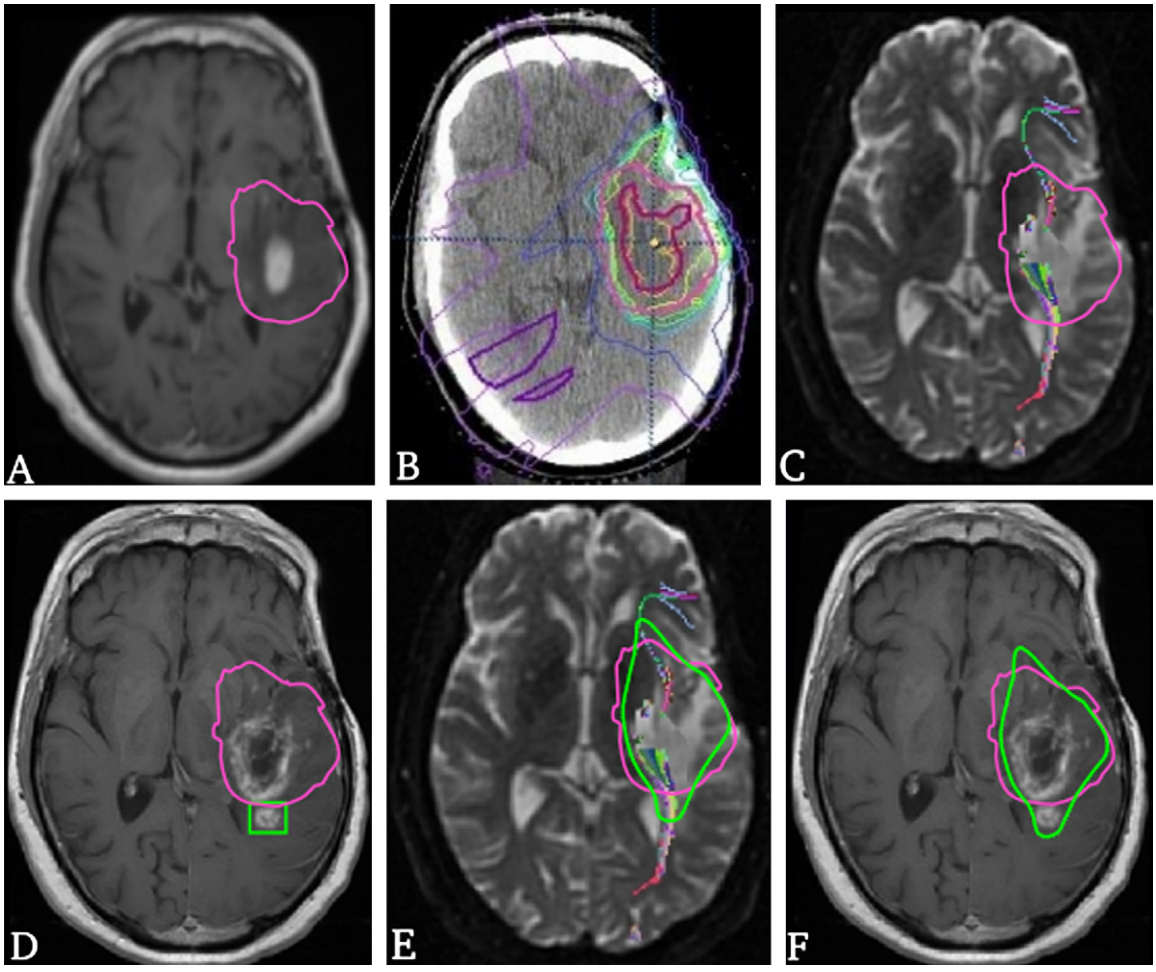


Fig. 4. (A) T1-weighted postcontrast image showing the primary anaplastic astrocytoma and treatment margin (pink line, 90% isodose) obtained from the treatment plan by computed tomography (B). (C) Diffusion tensor imaging reference image (b = 0) taken at the same time point showing all major diffusion paths passing through the tumor. Two major bundles pierce the treatment margin. (D) T1-weighted postcontrast image 3 months after the time point of (A) showing recurring tumor (green box) just outside of the treatment margin and in the same location as the major posterior bundle (C). (E) The treatment plan that was used for stereotactic radiotherapy (pink line) and the proposed anisotropic treatment plan (green line) with increased dose along the two prominent bundles emanating from the primary tumor and reduced margin along other directions. (F) Depiction of the original (pink) and proposed (green) treatment plans on the follow-up T1-weighted postcontrast image. Our contention is that the proposed plan might have stalled or may have even prevented the onset of the secondary tumor.

the cancer cells have migrated along the boundary of the ventricles in the subependyma (9) to the distant site in these patients. This route would explain the absence of any apparent diffusion paths from the primary tumor seen in Patient 4.

In Category 2 patients (local secondary tumor group), the secondary tumors were found very close to the treatment margin. Indeed, from many years of surgical resection, it has been shown that 95% of tumor progression occurs within 2–3 cm of the resection cavity (9). Thus modification of the treatment margin by 2–3 cm along the direction of higher diffusion tracts may have prevented these secondary tumors, as exhibited in Fig. 4F. Diffusion paths reconstructed from the primary tumor predicated both the location of tumor progression and also the spread of tumor in Category 3 patients (progression group). The results of Patients 12–14 demonstrate the ability of tractography to predict tumor spread locally. The imaging slice thickness used here of 3–6 mm may be too thick to discern fibers in the inferosuperior direction to the finite degree necessary; this may explain the absence of observable diffusion paths directly connecting the primary and secondary tumors in Patients 4, 5, and 11.

Most of the published works related to the use of DTI in tumor diagnosis, infiltration, and proliferation have directly used the scalar apparent diffusion coefficient or fractional anisotropy values (23–26). To the best of our knowledge, there have been no previous publications using DTI-based tractography for radiation planning or for follow-up evaluation of progressive disease (27). The results presented here suggest a direct and unique clinical utility for DTI tractography in SRT treatment planning. This is perhaps best exemplified by Fig. 4E, where we demonstrate a possible nonisotropic

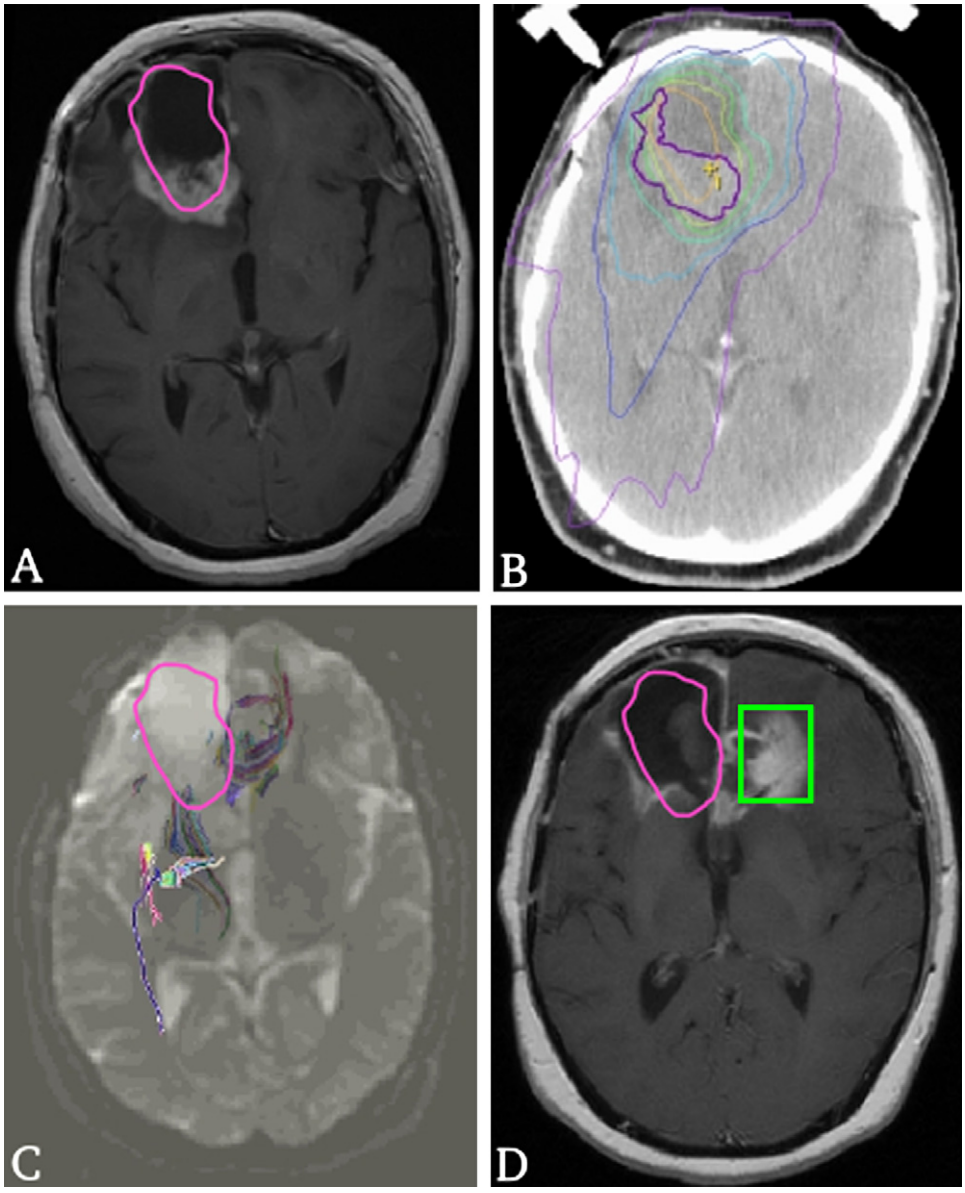


Fig. 5. (A) T1-weighted contrast image showing the primary glioblastoma multiforme and treatment margin (pink line = 90% isodose) obtained from the treatment plan by computed tomography (green line) (B). Surgical resection of the primary tumor (A) occurred approximately 10 months before the radiation treatment plan depicted in (B). (C) Diffusion tensor imaging reference image (b = 0) taken at the same time point (A), showing all diffusion paths passing through the tumor, the genu of corpus callosum, and internal capsule. (D) T1-weighted postcontrast image acquired 8 months after the time point of (A) showing progressive disease (green box) located just outside of the treatment margin, having spread along the genu of the corpus callosum as predicted in (C).

treatment margin based on DTI that encapsulates a secondary tumor that appeared in this patient (Patient 8) 3 months after completion of SRT using conventional isotropic treatment margins. Had the anisotropic margin been used, the microscopic infiltrating cells that led to this secondary tumor may have been eradicated at the time of the initial SRT treatment, thereby stalling or maybe even eliminating the onset of progressive disease.

Because of the infiltrative nature of gliomas, the resolution of conventional MR images is insufficient to accurately determine the microscopic tumor margin. When a standard isotropic treatment margin is used, excessive damage to normal brain tissue may occur in directions where infiltrative disease is absent. From the present analysis, our hypothesis that tumor cells migrate and spread microscopically along DTI paths appears to be valid. A large-scale prospective patient study is therefore warranted to better establish the correspondence between the microscopic spread of tumor cells and prominent paths of water diffusion leading from the primary tumor site. There are several potential advantages of conducting a prospective study following the current analysis. First, higher field MR systems (*e.g.*, 3T) and state-of-the art pulse sequences (*e.g.*, employing 60 or more directions of diffusion encoding) could be employed to improve DTI image quality

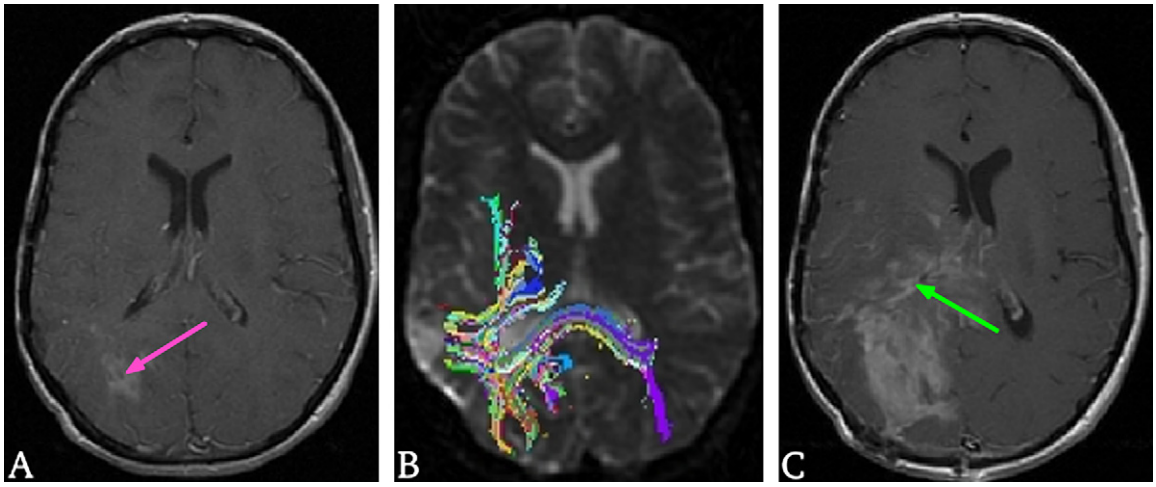


Fig. 6. (A) T1-weighted post-contrast image showing an astrocytoma (pink arrow). Surgical resection of the primary tumor occurred more than 2 years before the image (A). (B) Diffusion tensor imaging reference image (b = 0) take at the same time point (A), showing all diffusion paths passing through the tumor, the splenium of corpus callosum, and the internal capsule. (C) T1-weighted postcontrast image acquired 2 months after the time point (A) showing progressive disease (green arrow) having spread along the internal capsule and splenium of corpus callosum (B).

and resolution. Second, tractography could be performed immediately on acquisition of the DTI data and, in instances in which the diffusion-weighted image quality is deemed substandard, the patient could undergo a repeat imaging session early in the course of radiation therapy planning and treatment to obtain optimal DTI results. In 3 of the 14 datasets in the current study, the presence of edema immediately after surgical resection—and an associated decrease in fractional anisotropy values—precluded tractography analysis from the available DTI data. If afforded the opportunity for a subsequent DTI acquisition just before radiation treatment (which usually requires an MR image scan fused with a computed tomography scan for treatment planning), sufficient edema may have subsided to enable tractography to be performed. Third, with a larger patient pool, results could be correlated with specific cancer grade and type.

The following issues need to be investigated to improve the understanding of the relationship between tractography and tumor spread: tumor cells may migrate/diffuse differently than water molecules; tumor cells may interact with

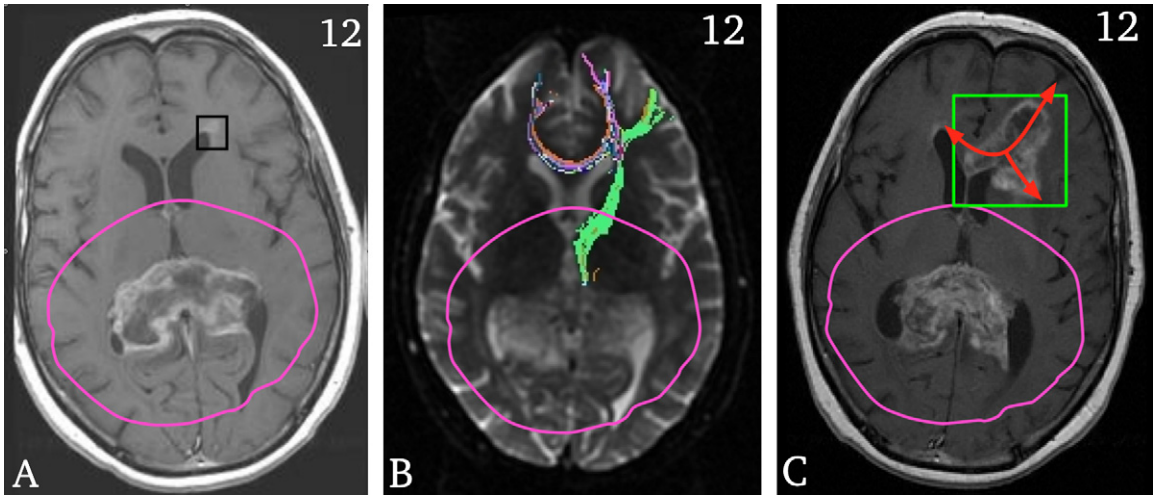


Fig. 7. (A) T1-weighted post-contrast magnetic resonance image acquired 6 months after stereotactic radiotherapy (SRT) in patient 1 (Fig. 1) showing a previously SRT-treated primary glioblastoma multiforme (GBM) in the splenium of corpus callosum and a small hyperintense region in the anterior horn of the left lateral ventricle (black box), which proved to be a secondary tumor (C). (B) For this special case, in which early onset of progression was identified, tractography was performed also at the site of progression. Shown is a diffusion tensor imaging (DTI) reference image (b = 0) at the time point (A) with a depiction of all tracts determined using DTIStudio emanating from the small hyper intense region in (A; black box). All of the three-dimensional tracts are projected onto the plane of the slice. (C) T1-weighted postcontrast image of the secondary tumor (green box) 3 months after the time point of (A), which occurred along the most prominent piercing tract in (B) and showing spread of the secondary tumor with substantial growth both laterally and anteriorly (red arrows). The 90% isodose volumes (SRT) are shown by pink lines in A–C.

neurons or chemicals in the brain in unexpected ways; there may be different types of tumor cells located in specific regions of the tumor (*i.e.*, migration may be dependent on the makeup of the tumor); and myelin may affect tumor cell migrations. To better address these effects, a more direct correlation between traditional histologic quantification of cell migration and DTI analysis is needed and this could be achieved using animal models (28).

## CONCLUSION

Our preliminary results on 14 patient datasets support the hypothesis that tractography by DTI is able to predict the pattern of microscopic tumor spread and treatment failure after conformal radiation. Future work will entail a more sophisticated analysis and prospective verification of the hypothesis that tumor cells migrate along paths of elevated water diffusion; achieved through the acquisition of additional MR DTI datasets and observations of tumor progression patterns in patients and through detailed histological analyses in animal models. Our goal is to demonstrate that anisotropic SRT treatment margins, optimized for each individual patient, can be used effectively and safely to reduce damage of normal brain tissue and at the same time stall or maybe even reduce the incidence of disease progression in these patients.

## REFERENCES


1. Ries LAG, Harkins D, Krapcho M, *et al*. SEER cancer statistics review, 1975–2003, National Cancer Institute. Bethesda, MD. Available at: http://seer.cancer.gov/csr/1975_2003. Based on November 2005 SEER data submission, posted to the SEER web site, 2006. Accessed November 20, 2006.
2. American Cancer Society. Treatment of specific types of brain and spinal cord tumors. Detailed guide: Brain/CNS tumors in adults, 2005. Available online at: http://www.cancer.org/docroot/CRI/content/CRI_2_4_4X_Treatment_of_Specific_Types_of_Brain_and_Spinal_Cord_Tumors_3.asp?rnav=cri. Accessed November 3, 2006.
3. Alexander E III, Moriarty TM, Davis RB, *et al*. Stereotactic radiosurgery for the definitive, noninvasive treatment of brain metastases. *J Natl Cancer Inst* 1995;87:34–40.
4. Kondziolka D, Patel A, Lunsford LD, *et al*. Stereotactic radiosurgery plus whole brain radiotherapy versus radiotherapy alone for patients with multiple brain metastases. *Int J Radiat Oncol Biol Phy* 1999;45:427–434.
5. Luxton G, Petrovich Z, Jozsef G, *et al*. Stereotactic radiosurgery: Principles and comparison of treatment methods. *Neurosurgery* 1993;32:241–259.
6. Petrovich Z, Yu C, Gianotta SL, *et al*. Survival and pattern of failure in brain metastasis treated with stereotactic gamma knife radiosurgery. *J Neurosurg* 2002;97(Suppl 5):499–506.
7. Hochberg FH, Pruitt A. Assumptions in the radiotherapy of glioblastoma. *Neurology* 1980;30:907–911.
8. Burger PC, Heinz ER, Shibata T, *et al*. Topographic anatomy and CT correlations in the untreated glioblastoma multiforme. *J Neurosurg* 1988;68:698–704.
9. Giese A, Bjerkviq R, Berens ME, *et al*. Cost of migration: Invasion of malignant gliomas and implications for treatment. *J Clin Oncol* 2003;21:1624–1636.
10. Johnson PC, Hunt SJ, Drayer BP. Human cerebral gliomas: Correlation of postmortem MR imaging and neuropathologic findings. *Radiology* 1989;170:211–217.
11. Matsukado Y, MacCarty CS, Kernohan JW. The growth of glioblastoma multiforme (astrocytomas, grades 3 and 4) in neurosurgical practice. *J Neurosurg* 1961;18:636–644.
12. Jacobsen CT, Miller RH. Control of astrocyte migration in the developing cerebral cortex. *Dev Neurosci* 2003;25:207–216.
13. Basser PJ, Pajevic S, Pierpaoli C, *et al*. In vivo fiber tractography using DT-MRI data. *Magn Reson Med* 2000;44:625–632.
14. Behrens TE, Woolrich MW, Jenkinson M, *et al*. Characterization and propagation of uncertainty in diffusion weighted MR imaging. *Magn Reson Med* 2003;50:1077–1088.
15. Campbell JS, Siddiqi K, Rymar VV, *et al*. Flow-based fiber tracking with diffusion tensor and Q-ball data: Validation and comparison to principal diffusion direction techniques. *NeuroImage* 2005;27:725–736.
16. Catani M, Howard RJ, Pajevic S, *et al*. Virtual in vivo interactive dissection of white matter fasciculi in the human brain. *NeuroImage* 2002;17:77–94.
17. Hagmann P, Thiran JP, Jonasson L, *et al*. DTI mapping of human brain connectivity: Statistical fibre tracking and virtual dissection. *NeuroImage* 2003;19:545–554.
18. Huang H, Zhang J, van Zijl PC, *et al*. Analysis of noise effects on DTI-based tractography using the brute-force and multi-ROI approach. *Magn Reson Med* 2004;52:559–565.
19. Parker GJM, Wheeler-Kingshott CA, Barker GJ. Estimating distributed anatomical connectivity using fast marching methods and diffusion tensor imaging. *IEEE Trans Med Imaging* 2002;21:505–512.
20. Parker GJM, Haroon HA, Wheeler-Kingshott CA. A framework for a streamline-based probabilistic index of connectivity (PICo) using a structural interpretation of MRI diffusion measurements. *J Magn Reson Imaging* 2003;18:242–254.
21. Tournier JD, Calamante F, Gadian DG, *et al*. Diffusion weighted magnetic resonance imaging fibre tracking using a front evolution algorithm. *NeuroImage* 2003;20:276–288.
22. Zhang J, Zijl Van, Lattera J, *et al*. Unique patterns of diffusion directionality in rat brain tumors revealed by high-resolution diffusion tensor MRI. *Magn Reson Med* 2007;58:454–462.
23. Beppu T, Inoue T, Shibata Y, *et al*. Fractional anisotropy value by diffusion tensor magnetic resonance imaging as a predictor of cell density and proliferation activity of glioblastomas. *Surg Neurol* 2005;63:56–61.
24. Hein PA, Eskey CJ, Dunn JF, *et al*. Diffusion-weighted imaging in the follow-up of treated high-grade gliomas: Tumor recurrence versus radiation injury. *AJNR Am J Neuroradiol* 2004;25:201–209.
25. Laundre BJ, Jellison BJ, Badie B, *et al*. Diffusion tensor imaging of the corticospinal tract before and after mass resection as correlated with clinical motor findings: Preliminary data. *AJNR Am J Neuroradiol* 2005;26:791–796.
26. Price SJ, Burnet NG, Donovan T, *et al*. Diffusion tensor imaging of brain tumors at 3T: A potential tool for assessing white matter tract invasion? *Clin Radiol* 2003;58:455–462.
27. Field AS, Alexander AL. Diffusion tensor imaging in cerebral tumor diagnosis and therapy. *Top Magn Reson Imaging* 2004;15:315–324.
28. van Furth WR, Laughlin S, Taylor MD, *et al*. Imaging of murine brain tumors using a 1.5 Tesla clinical MRI system. *Can J Neurol Sci* 2003;30:326–332.